

Thermal Parameters and Microstructural Development in Directionally Solidified Zn-Rich Zn-Mg Alloys



TALITA A. VIDA, EMMANUELLE S. FREITAS, CRYSTOPHER BRITO,
NOÉ CHEUNG, MARIA A. ARENAS, ANA CONDE, JUAN DE DAMBORENEA,
and AMAURI GARCIA

Transient directional solidification experiments have been carried out with Zn-Mg hypoeutectic alloys under an extensive range of cooling rates with a view to analyzing the evolution of microstructure. It is shown that the microstructure is formed by a Zn-rich matrix of different morphologies and competitive eutectic mixtures ($Zn-Zn_{11}Mg_2$ and $Zn-Zn_2Mg$). For 0.3 wt-pct Mg and 0.5 wt-pct Mg alloys, the Zn-rich matrix is shown to be characterized by high-cooling rates plate-like cells (cooling rates >9.5 and 24 K/s, respectively), followed by a granular-dendritic morphological transition for lower cooling rates. In contrast, a directionally solidified Zn1.2 wt-pct Mg alloy casting is shown to have the Zn-rich matrix formed only by dendritic equiaxed grains. Experimental growth laws are proposed relating the plate-like cellular interphase, the secondary dendritic arm spacing, and the eutectic interphase spacings to solidification thermal parameters, *i.e.*, cooling rate and growth rate. The experimental law for the growth of secondary dendritic spacings under unsteady-state solidifications is also shown to encompass results of hypoeutectic Zn-Mg alloys subjected to steady-state Bridgman growth.

DOI: 10.1007/s11661-016-3494-7

© The Minerals, Metals & Materials Society and ASM International 2016

I. INTRODUCTION

THE addition of Mg to improve corrosion stability of Zn coatings is a technologically common practice for corrosion protection of products of use in the civil and automotive industries.^[1–8] Despite the fact that Mg is less noble than Zn, the role of Zn-Mg intermetallics on the corrosion performance has been the subject of a number of recent studies in the literature with a view to investigating specific mechanisms, which have not yet been explained.^[9–14]

Vlot *et al.* examined the corrosion behavior of Zn-Mg alloys in the range of compositions 1.5–2.0 wt-pct Mg, characterized by microstructures formed by Zn grains surrounded by a eutectic mixture of $Zn/MgZn_2$ and reported a period of roast formation up to 20 times higher than that of a reference hot dip galvanized coating.^[1] Dutta *et al.* carried out hot dip experiments with Zn-0.5 wt-pct Mg and Zn-2.5 wt-pct Mg alloys and reported that both hardness of the top surface of the

coatings and the resulting corrosion resistance were higher than those attained in a pure Zn bath.^[4] Yao *et al.* conducted an experimental study with Zn-Mg coatings having from 1 to 4 wt-pct Mg and reported improved anticorrosion properties of the Zn-3 wt-pct Mg coatings when compared with a pure Zn coating, as well as with a significant increase in hardness.^[7]

Zn and Mg are also considered potential elements regarding biodegradable bone-implant applications. Mg alloys have mechanical properties close to those of bone; however, corrosion rates accompanied by hydrogen release are conducive to high degradation rates. Zn is a biologically tolerable element even when alloyed to Mg (up to 50 pct Mg), which makes Zn-Mg alloys potential alternatives as biodegradable materials. Furthermore, Zn has a much lower corrosion rate in physiological solutions when compared with Mg. Despite the lack of systematic studies concerning the behavior of Zn-rich Zn-Mg alloys in biological environments, it is known that such alloys have other important characteristics such as lower melting points and better machinability when compared with Mg.^[15–24]

It is well known that microstructural features play a significant role on mechanical and corrosion properties of metallic alloys.^[25–34] Despite the potential of applications of Zn-Mg alloys, the literature is scarce on studies of microstructural characterization of these alloys, mainly with focus on structure-properties correlations. Liu and Jones carried out an extensive study on solidification microstructure selection of Zn-Mg alloys (alloys from 1.08 to 5.04 wt-pct Mg) by controlled growth of samples from the melt, using a Bridgman-type

TALITA A. VIDA, Ph.D. Student, EMMANUELLE S. FREITAS, Researcher, and NOÉ CHEUNG and AMAURI GARCIA, Professors, are with the Department of Manufacturing and Materials Engineering, University of Campinas, Mendeliev Street 200, Campinas, SP 13083-860, Brazil. Contact email: cheung@fem.unicamp.br CRYSTOPHER BRITO, Professor, is with the Marine Institute, Federal University of São Paulo, Alm. Saldanha da Gama Avenue 88, Santos, SP 11030-400, Brazil. MARIA A. ARENAS and ANA CONDE, Researchers, and JUAN DE DAMBORENEA, Professor, are with the National Center for Metallurgical Research (CENIM-CSIC), Avda Gregorio del Amo 8, 28040 Madrid, Spain.

Manuscript submitted July 22, 2015.

Article published online April 8, 2016

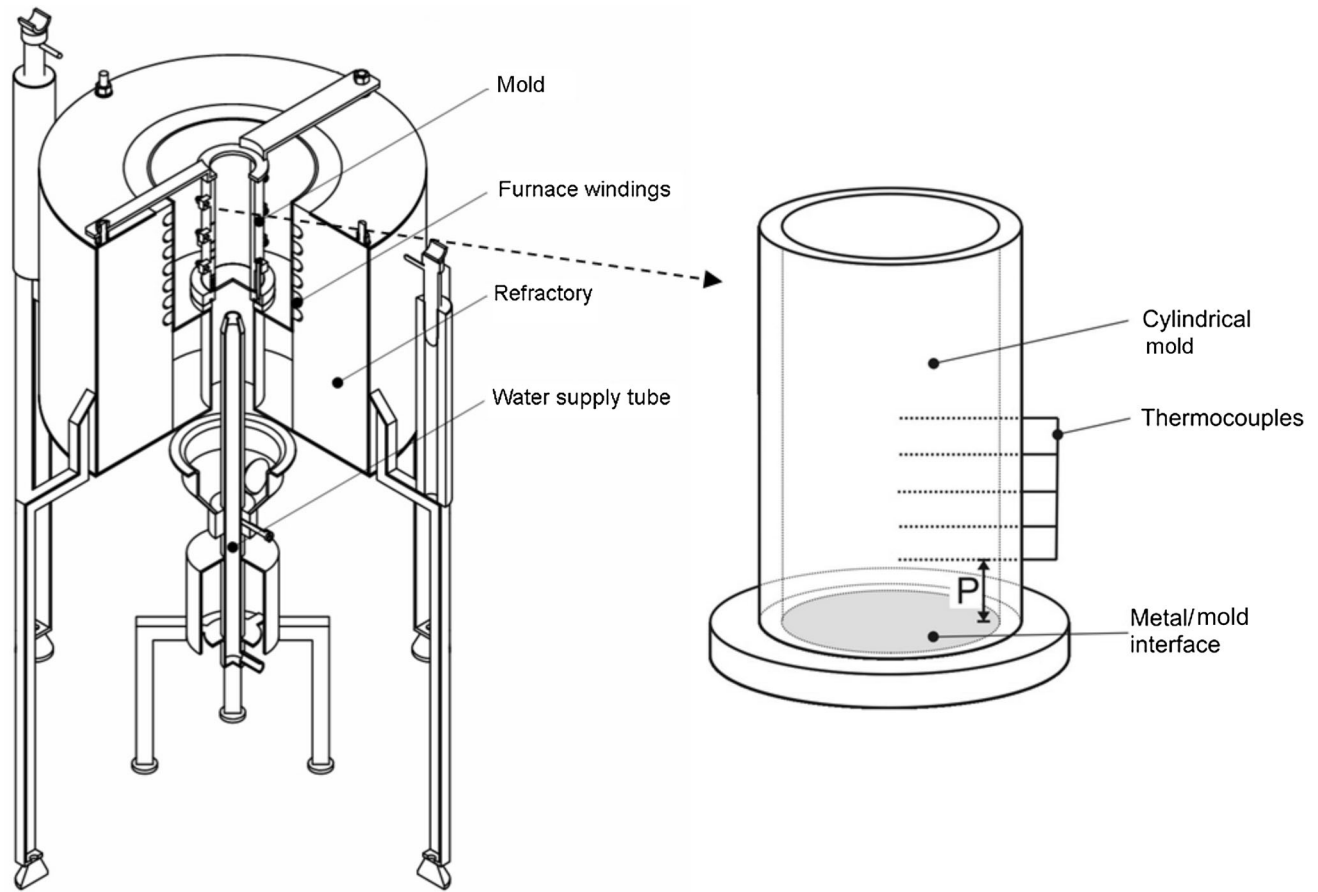


Fig. 1—Schematic vertical upward directional solidification casting assembly and mold details.

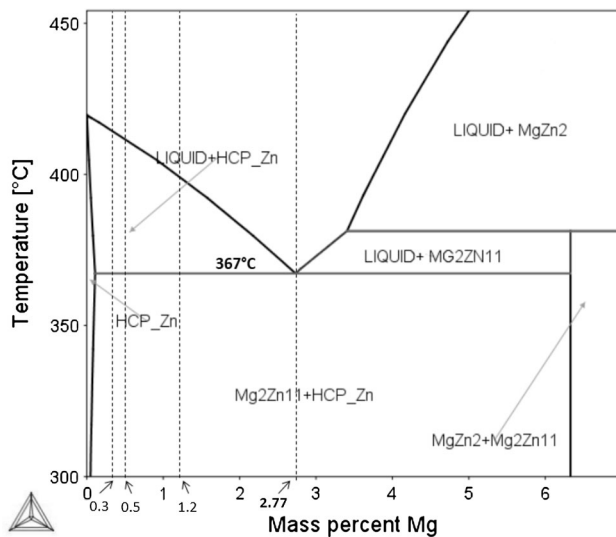


Fig. 2—Partial Zn-Mg phase diagram with indications of alloys analyzed in the present study.

steady-state solidification apparatus.^[35,36] They used a constant thermal gradient of 15 K/mm and growth rates varying from 0.001 to 1 mm/s. These authors carried out also experiments with samples that were cast into a wedge-section copper mold and solidified at growth

rates from 1 to 8 mm/s. They reported the occurrence of a dendritic primary Zn-rich phase and a wide range of eutectic morphologies (rod-like, spherulitic, spiral). Yao *et al.*^[24] examined experimentally the effects of Mg on the microstructure of Zn-Mg alloys (1-5 wt-pct Mg) by pouring the alloys samples from the melt in a permanent mold, under argon atmosphere. The cooling parameters were not quantified, and only a qualitative description of the resulting microstructures is reported. Krieg *et al.*^[11] characterized the microstructures of Zn-Mg alloys, with Mg content varying from 1 to 3 wt pct, from samples cooled down from the melt by exposure to room temperature. The only quantitative parameter associated with each sample was the solidification time, which varied from 1 to 8 minutes. They evaluated the corrosion resistance based on the alloy Mg content and on the fineness of the microstructure, and concluded that the Mg content is not the main parameter enhancing the corrosion behavior, but rather the main role was shown to be exerted by the fineness of the microstructure. However, despite the important role that the scale of the microstructure plays on the corrosion resistance of Zn-Mg alloys, the literature is scarce in systematic investigations relating microstructural parameters to thermal parameters of transient solidification, which is typical of industrial casting processes where both the thermal gradient and growth rate are interdependent and vary freely with time.^[37-46]

Table I. Chemical Composition (Wt Pct) of Metals Used to Prepare the Alloys

Element	Zn	Mg	Mn	Cr	Fe	Al	Pb	Si
Zn	balance	—	—	—	0.015	—	0.012	0.003
Mg	0.01	balance	0.01	0.01	0.01	0.11	—	—

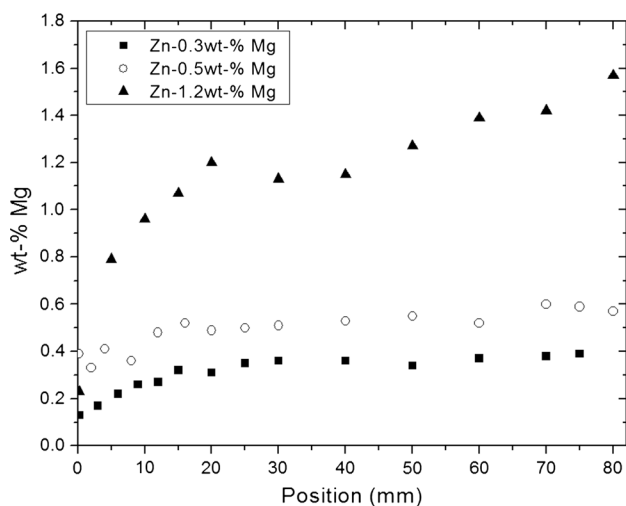


Fig. 3—Mg profiles along the DS castings length.

The present study aims to contribute to a quantitative characterization of thermal and structural features in the transient solidification of hypoeutectic Zn-Mg alloys. Taking into account the previous studies on Zn-Mg alloys from the literature, the present investigation aims to complement the existing results focusing on dilute Zn-Mg alloys with a view to analyzing macrostructure and microstructure evolution. A water-cooled directional solidification apparatus will be used, which permits a wide range of operational growth rates and cooling rates to be examined along the entire length of the directionally solidified (DS) casting. This will permit to evaluate the development of the phases forming the alloy microstructures and eventual morphological transitions, and to establish correlations between quantitative parameters, such as interphase spacings and local solidification thermal parameters.

II. EXPERIMENTAL PROCEDURE

A directional solidification setup (shown schematically in Figure 1) was used so that heat was directionally extracted only through a water-cooled bottom made of low carbon steel promoting vertical upward transient directional solidification. Details about the solidification apparatus used in the present study have been described in previous studies.^[43,47,48] The experiments were carried out with hypoeutectic Zn-Mg alloys having the following nominal compositions: Zn-0.3 wt-pct Mg; Zn-0.5 wt-pct Mg and Zn-1.2 wt-pct Mg alloys, as

indicated in the partial Zn-Mg phase diagram calculated by the Thermo-Calc software and depicted in Figure 2. The chemical compositions of metals used to prepare these alloys are shown in Table I.

The alloys were prepared using alloying elements in a fixed proportion, which were melted in a refractory crucible in a muffle furnace heated by Kanthal A1 heating elements, under argon atmosphere. Zn was melted first and then elemental Mg pieces were added to the melt. Both metal components were mixed well and allowed remelt further for three times to guarantee homogenization. The molten alloy was then poured into the casting chamber of the directional solidification apparatus, which was subjected to a forced argon gas flow to avoid oxidation and loss of Zn and Mg. The hypoeutectic Zn-Mg alloys were melted *in situ* by controlling the power of the radial electrical wiring. Three solidification experiments were carried out with each alloy composition with a view to verifying the reproducibility of the directional solidification system, permitting a triplicate analysis on the evolution of cooling curves along the length of the DS castings to be carried out. More details on the solidification experiment and temperature measurements can be found in a recent study on Mg-Zn alloys.^[49]

An etching solution (Nital 10 pct reagent) applied during 7 seconds was used to reveal the microstructures. The optical microscopy was performed using an Olympus Inverted Metallurgical Microscope (model 41GX). The cellular (λ) and secondary dendritic arm (λ_2) spacings were measured from the optical images of the solidified samples on longitudinal sections of the castings (about 40 independent readings for each selected position, with the average taken to be the local spacing). Microstructural characterization was complemented by the use of a ZEISS scanning electron microscope—SEM (ZEISS-EVO-MA15), equipped with an energy dispersive spectroscope—EDS (OXFORD-X-MAX). The interlamellar spacing of the eutectic mixture was measured from SEM images.

Some samples of each DS alloy casting were selected and subjected to X-ray diffraction (XRD) analyses. The patterns were obtained by a XRD diffractometer with a 2-theta range from 10 deg to 90 deg, Cu-K α radiation with a wavelength, λ , of 0.15406 nm, with a view to determining all the phases forming the microstructures.

Samples for segregation analysis were extracted along different positions from the cooled surface of the casting and measured by a fluorescence spectrometer (FRX), Shimadzu EDX-720 model, to estimate local average concentrations through an area of 100 mm² probe.

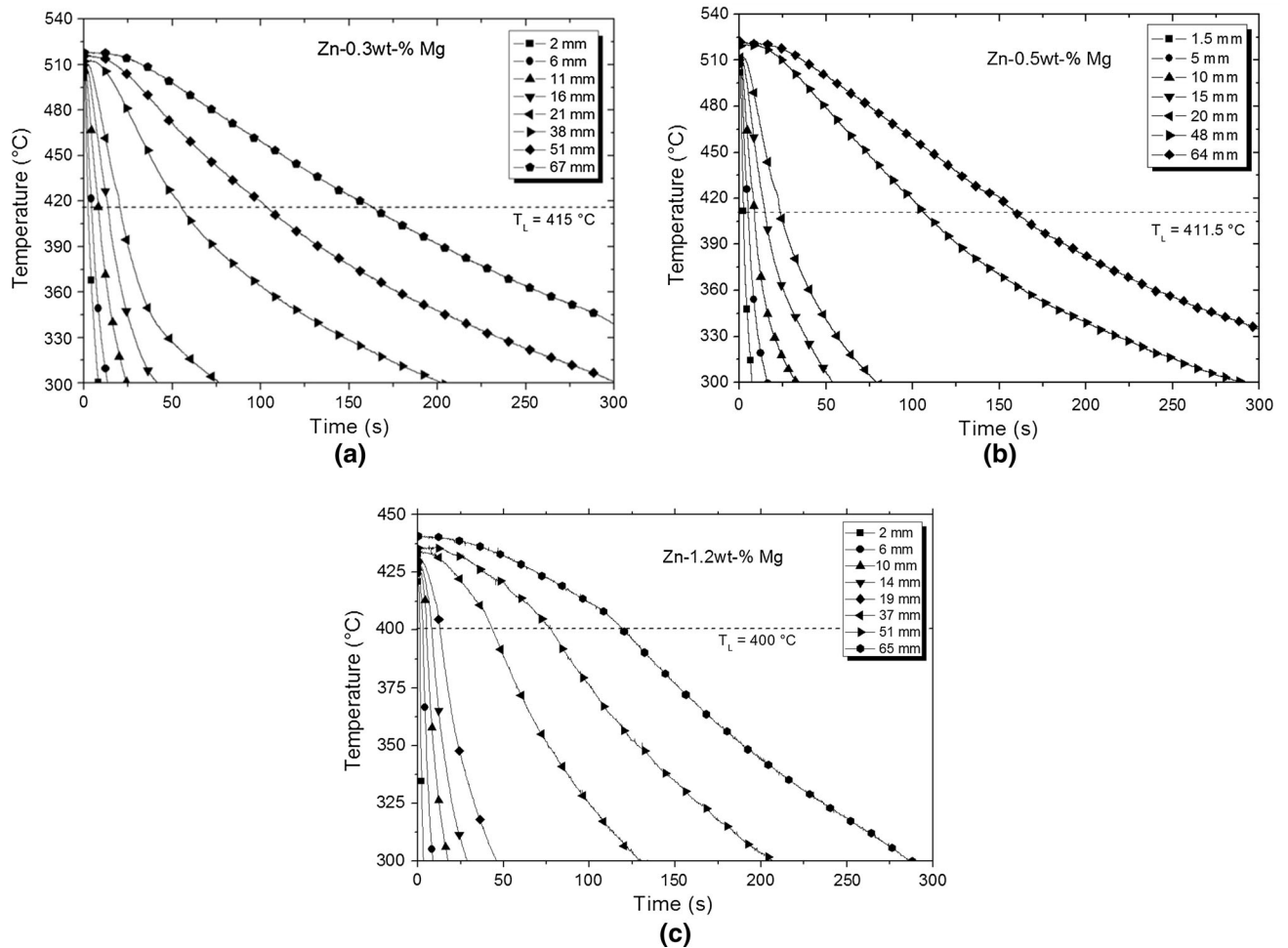


Fig. 4—Experimental cooling curves for different positions in the DS castings: (a) Zn-0.3 wt-pct Mg; (b) Zn-0.5 wt-pct Mg; and (c) Zn-1.2 wt-pct Mg.

III. RESULTS AND DISCUSSION

A. Chemical Analysis and Solidification Thermal Parameters

Figure 3 shows the experimental Mg-concentration profiles, determined along the length of DS castings as a function of position (P) from the cooled surface of the casting ($P = 0$). For any alloy examined, the observed trend is that of a normal segregation profile for a distribution coefficient (k) < 1 . Mg is rejected at the solid/liquid interface during the evolution of solidification enriching the molten liquid. Since Mg is much less dense than Zn, this Mg-rich liquid would tend to move toward the open liquid in the DS casting (opposite path with respect to the gravity vector), while the solidification progresses vertically upwards. This effect is noticeable only for the higher Mg content alloy (Zn-1.2 wt-pct Mg).

Figure 4 depicts the experimental cooling curves collected from thermocouples placed in different positions along the geometrical center of the cylindrical mold cavity, for each alloy examined. These cooling curves have been used to generate plots of position (P) in casting (from the cooled bottom of the casting) vs the time associated with the passage of the *liquidus* isotherm

by each thermocouple, as shown in Figure 5(a). The derivatives of these functions with respect to time gave values for the growth rate (V), as shown in Figure 5(b). It can be seen that the same experimental growth law can represent the kinetics of solidification of the Zn0.3 wt-pct Mg and Zn0.5 wt-pct Mg alloys. The cooling rate (\dot{T}) was determined along the castings lengths, by considering the thermal data recorded immediately after the passage of the *liquidus* isotherm by each thermocouple. The resulting experimental \dot{T} values are shown in Figure 5(c), where a large spectrum of cooling rates can be observed. The thermal gradient, G , is shown in Figure 5(d) as a function of (P) from the cooled bottom of the DS casting. It has been obtained from the relationship between the cooling rate (\dot{T}) and the growth rate (V), namely $\dot{T} = G.V$. It can be seen that the G profile is lower for the 1.2 wt-pct Mg when compared with that of the dilute alloys (0.3 wt-pct Mg/0.5 wt-pct Mg). However, an opposite behavior is shown in Figure 5(b) regarding the experimental $V = f(P)$ profiles, *i.e.*, the lower V profile is that of the dilute alloys. This has led to a constant experimental cooling rate profile as shown in Figure 5(c), where a

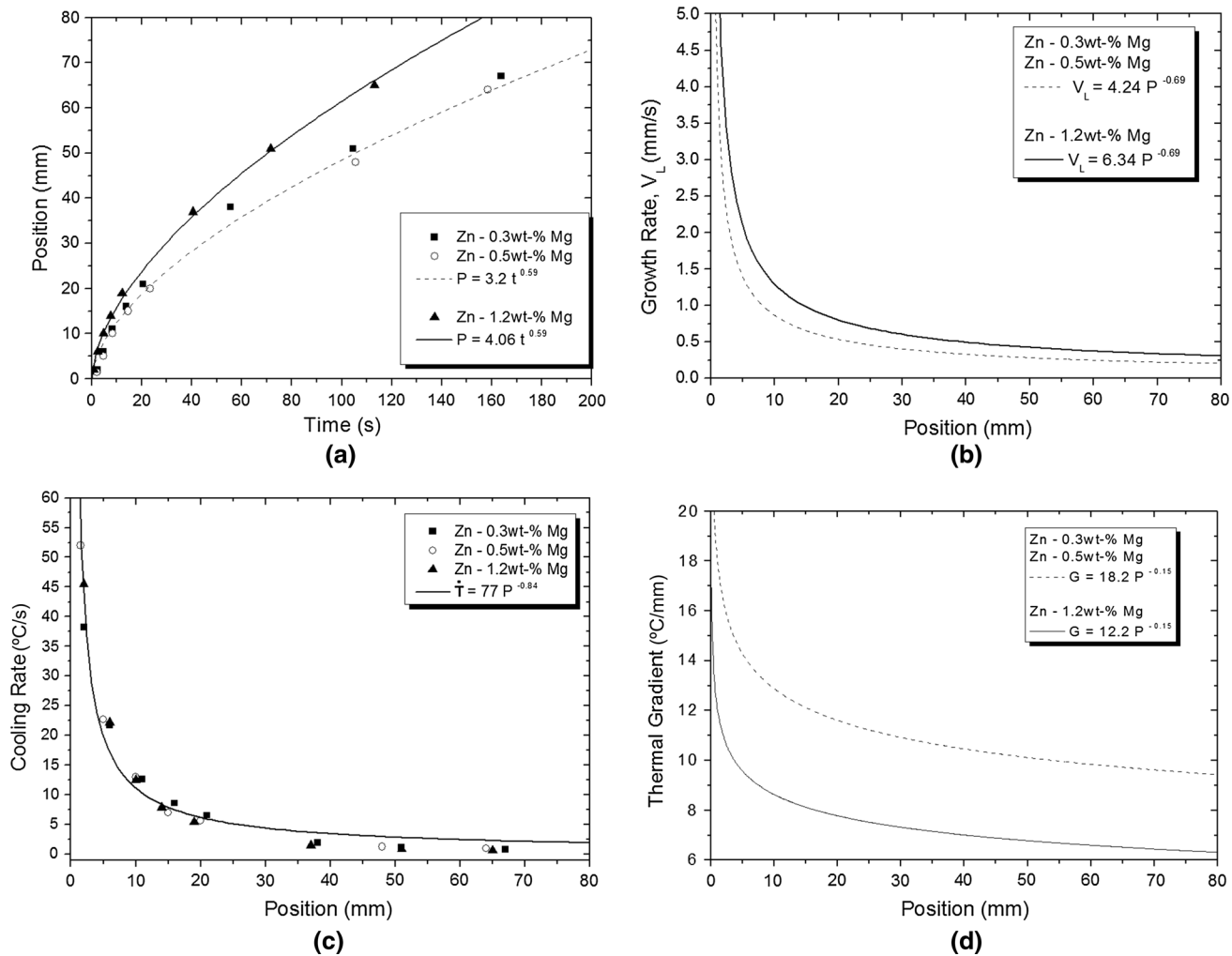


Fig. 5—(a) Position in casting (P) from the cooled bottom vs time associated with the passage of the *liquidus* isotherm; (b) growth rate as function of P ; (c) cooling rate as a function of P ; (d) thermal gradient as a function of P .

same experimental $\dot{T} = f(P)$ law applies to all the three alloys examined.

B. Macrostructure and Microstructure

A Zn-rich matrix of different morphologies characterizes the microstructures along the DS casting for the three alloys examined. The secondary phases were identified by XRD analysis and are shown in Figure 6, and include the following intermetallic compounds (IMCs): $Zn_{11}Mg_2$, and Zn_2Mg , which were also expected according to the simulated phase diagram shown in Figure 2. Very similar 2θ peaks associated with the phases are shown in Figure 6. These IMCs are present in the binary eutectic mixture, and Zn-rich Zn-Mg system is known to exhibit two kinds of competitive eutectic mixture,^[35] *i.e.*, Zn- $Zn_{11}Mg_2$ and Zn- Zn_2Mg that can be observed concurrently all along the DS castings.

Complementarily to the XRD analysis, EDS measurements were performed in some positions ($P = 15$ and 50 mm) of the DS Zn-0.5 wt-pct Mg and Zn-1.2 wt-pct Mg alloys castings (Figure 7). The

Zn-0.3 wt-pct Mg alloy was not subjected to EDS because its Mg content is close to that of the Zn-0.5 wt-pct Mg alloy. In the EDS analysis, the stoichiometry of $(Zn_{11}Mg_2)$ phase was not an exact 5.5:1 ratio between Zn and Mg atoms, because of interferences due to unavoidable interactions between the X-ray beam and the bulk Zn matrix. However, the identification of the $(Zn_{11}Mg_2)$ phase in this study has been confirmed by the approximate ratio between Mg and Zn atoms shown in the results presented in Table II. A similar argument could be extended to the identification of the (Zn_2Mg) phase, *i.e.*, by the 2:1 ratio between the Mg and Zn atoms also shown in Table II.

In Figure 8 (Zn-0.3 wt-pct Mg alloy) and Figure 9 (Zn-0.5 wt-pct Mg alloy), it can be seen that the resulting DS macrostructures are characterized by fine columnar grains aligned with the heat flow direction close to the bottom of the casting, followed by fine equiaxed grains up to the top of the castings. The columnar to equiaxed transitions (CET) occurred at about 9.5 and 24 K/s for the Zn-0.3 wt-pct Mg and Zn-0.5 wt-pct Mg alloys, respectively. No evidence of a single critical cooling rate determining the CET for

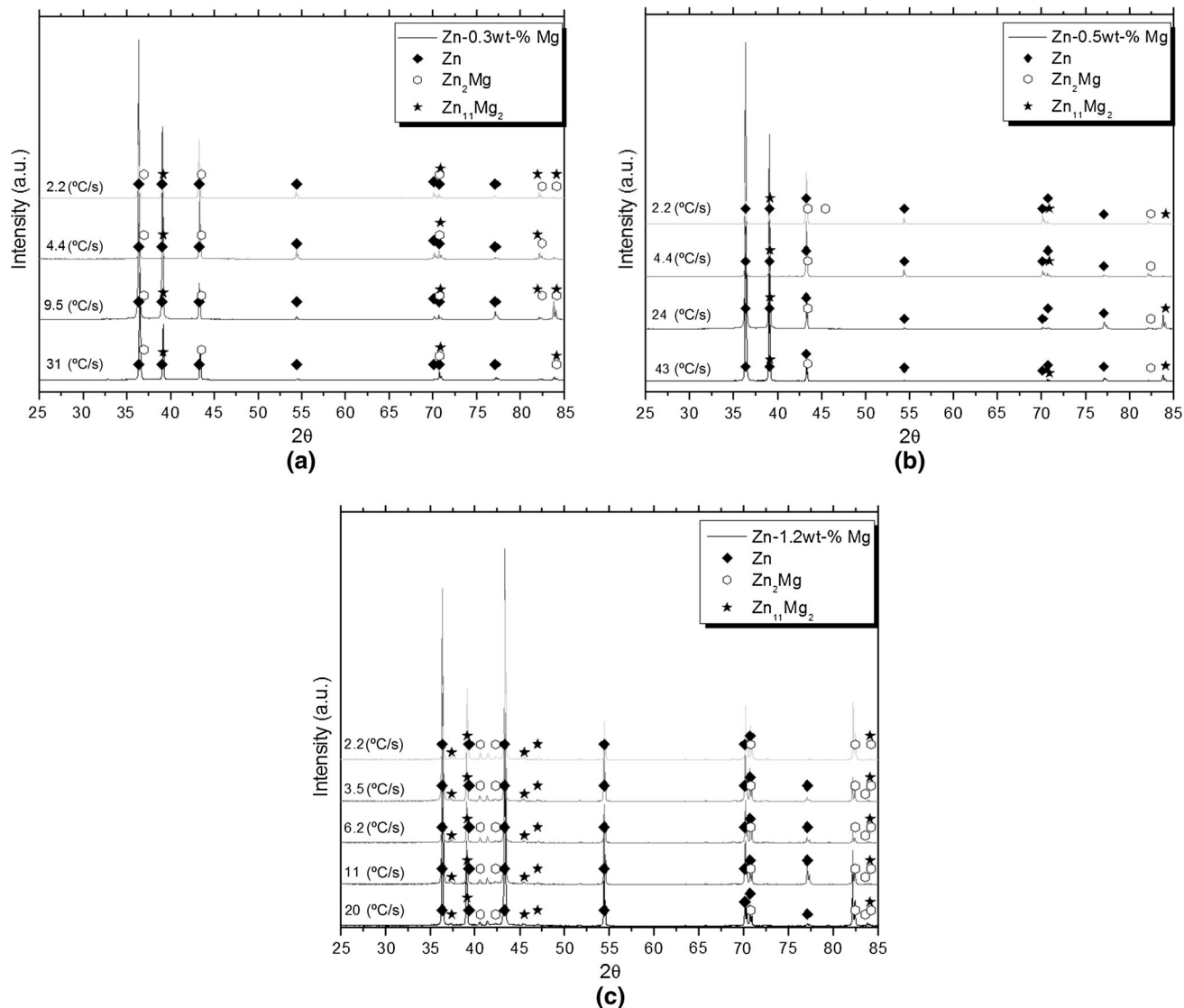


Fig. 6—X-ray diffraction (XRD) patterns of (a) Zn-0.3 wt-pct Mg, (b) Zn-0.5 wt-pct Mg, and (c) Zn-1.2 wt-pct Mg samples that solidified under different cooling rates along the DS castings length.

hypoeutectic alloys, as suggested in the literature for hypoeutectic Sn-Pb and Al-Cu alloys,^[50] could be found. The literature also reports that high cooling rates favor the formation of columnar macrostructures.^[51,52] However, the macrostructure of the Zn1.2 wt-pct Mg alloy is entirely formed by fine equiaxed grains, as shown in Figure 10, even for regions close to the cooled surface of the casting that are associated with higher cooling rates. It seems that despite the slight increase in the alloy Mg, the nucleation frequency is positively favored inducing a copious nucleation ahead the solidification front promoting the growth of equiaxed grains along the entire length of the DS casting. According to a recent study,^[53] Zn₂Mg particles act as potent heterogeneous nucleation sites. Even with slight increase in the Mg content, the grain refiner effect of the MgZn₂ particles associated with the solute effect of Mg on restricting grain growth makes both cooperative factors responsible for the

dominant equiaxed morphology in the Zn-Mg DS castings.

A particular Zn-rich plate-like cellular microstructure is associated with the columnar regions of both DS Zn0.3 wt-pct Mg and Zn0.5 wt-pct Mg castings. Despite the non-equilibrium solidification conditions, these plate-like cells seem to grow side by side and in a coupled way with the eutectic mixture during the directional growth, resembling a eutectic-like lamellar growth. Actually, these cells can be classified as high-cooling rate cells, as similarly reported in a recent study on the microstructural evolution of an Al-Mg-Si alloy.^[54] The morphology of the solidification front changes from planar to cellular and then to dendritic with the increase in V , defining a direct effect of solidification thermal parameters on the microstructural morphology. Further increase in V changes the dendritic front back to cellular and planar front, defining a

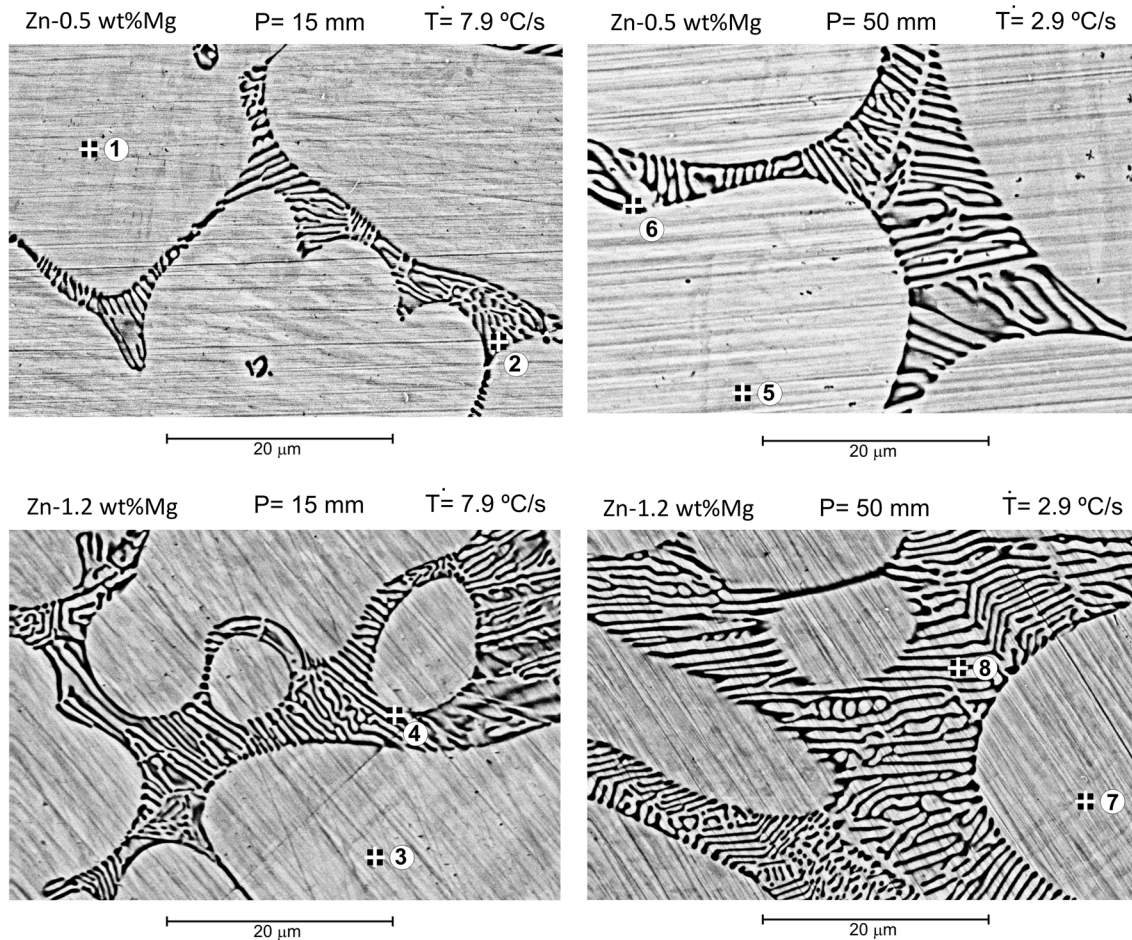


Fig. 7—Typical SEM morphology of the Zn-based intermetallic phases for two positions ($P = 15$ and 50 mm) and two alloys (Zn-0.5 wt pct Mg and Zn-1.2 wt pct Mg) showing some locations of EDS analysis.

Table II. Composition of the Intermetallic Phases Obtained by EDS in a SEM for Zn-0.5 Wt-Pct Mg and Zn-1.2 Wt-Pct Mg Alloys

Measurement Position	Mg (At. Pct)	Zn (At. Pct)	Phase Identification
1	0	100	Zn
2	14.54	85.46	$Zn_{11}Mg_2$
3	0	100	Zn
4	17.44	82.56	$Zn_{11}Mg_2$
5	0	100	Zn
6	28.04	71.96	Zn_2Mg
7	0.96	99.04	Zn
8	16.76	83.74	$Zn_{11}Mg_2$

reverse transition that gives rise to the so-called high-velocity cells (or high-cooling rate cells for transient solidification conditions) and a planar solid/liquid interface associated with the limit of absolute stability.^[55–57] Despite the wide range of microstructural eutectic morphologies reported in the study by Liu and Jones^[35] on Zn-Mg alloys, no mention was made of the occurrence of Zn-rich plate-like cellular microstructures, with the Zn-rich matrix being reported as having a dendritic morphology. However, a number of

investigations on Zn-based alloys^[58–61] reported the occurrence of high-velocity plate-like cells in steady-state Bridgman-grown samples, which were shown to be associated with rapid solidification conditions of dilute Zn-Cu^[58,59] and Zn-Ag alloys.^[60,61] For unsteady-state solidification conditions plate-like cells were shown to occur for a Zn 2.2 wt-pct Cu alloy only for $\dot{T} > 16$ K/s,^[62] for a Zn 0.8 wt-pct Ag alloy^[63] for $\dot{T} > 10$ K/s, and for Zn-10 wt-pct Sn and Zn-20 wt-pct Sn solder alloys in a range of cooling rates from 0.3 to 45 K/s.^[64,65]

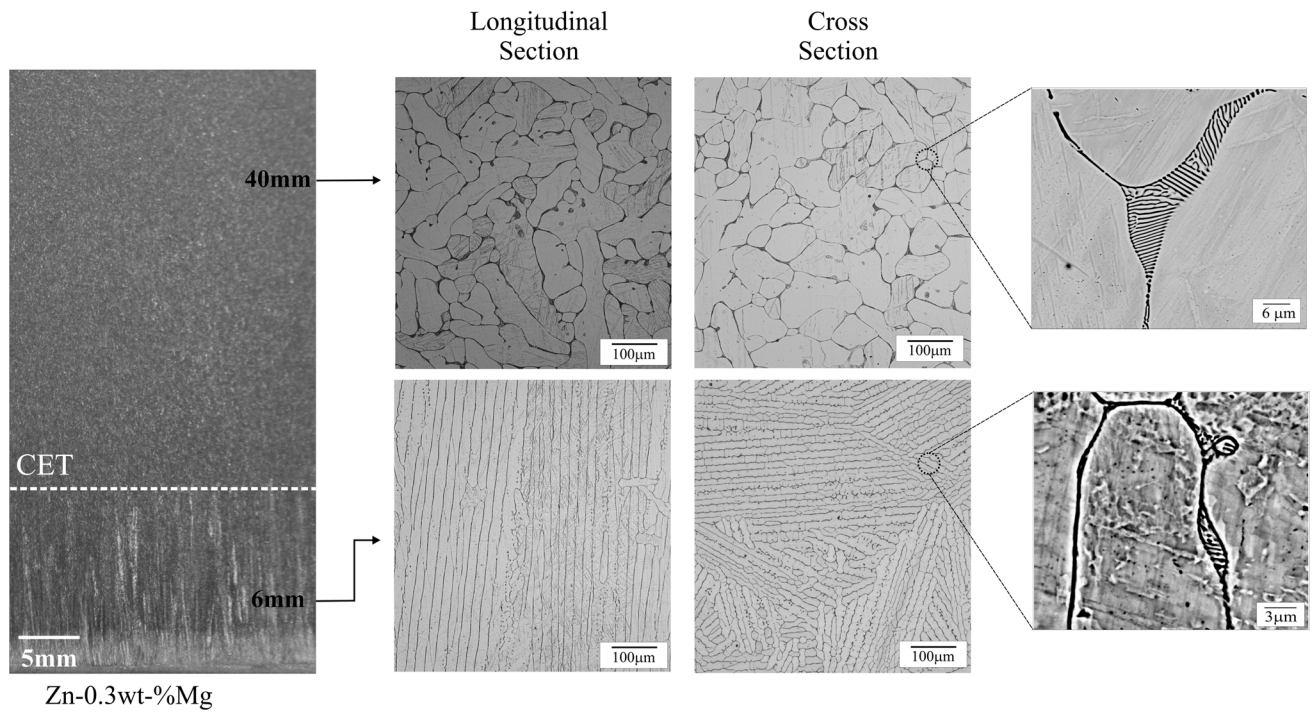


Fig. 8—Macrostructure and typical microstructures along the DS Zn-0.3 wt-pct Mg casting.

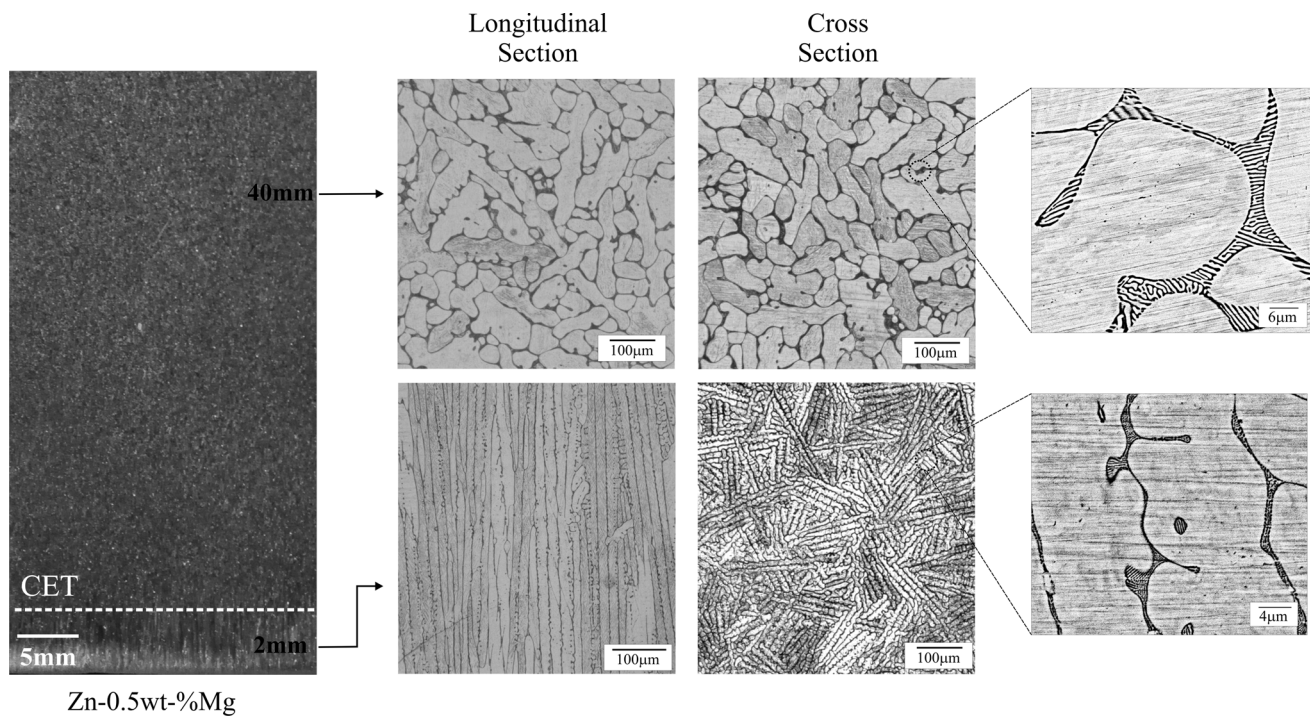


Fig. 9—Macrostructure and typical microstructures along the DS Zn-0.5 wt-pct Mg casting.

In the present study, after the columnar to equiaxed transition in the Zn0.3Mg and Zn0.5 wt-pct Mg DS castings, the Zn-rich equiaxed grains change gradually from a granular aspect to a more complex morphology with the onset of lateral instabilities typical of secondary

dendritic branches, as shown in the longitudinal section of Figure 9 (defining a morphological transition region along the castings length). In contrast, in the Zn1.2 wt-pct Mg DS casting, the Zn-rich matrix has a clear dendritic morphology from the bottom to the top

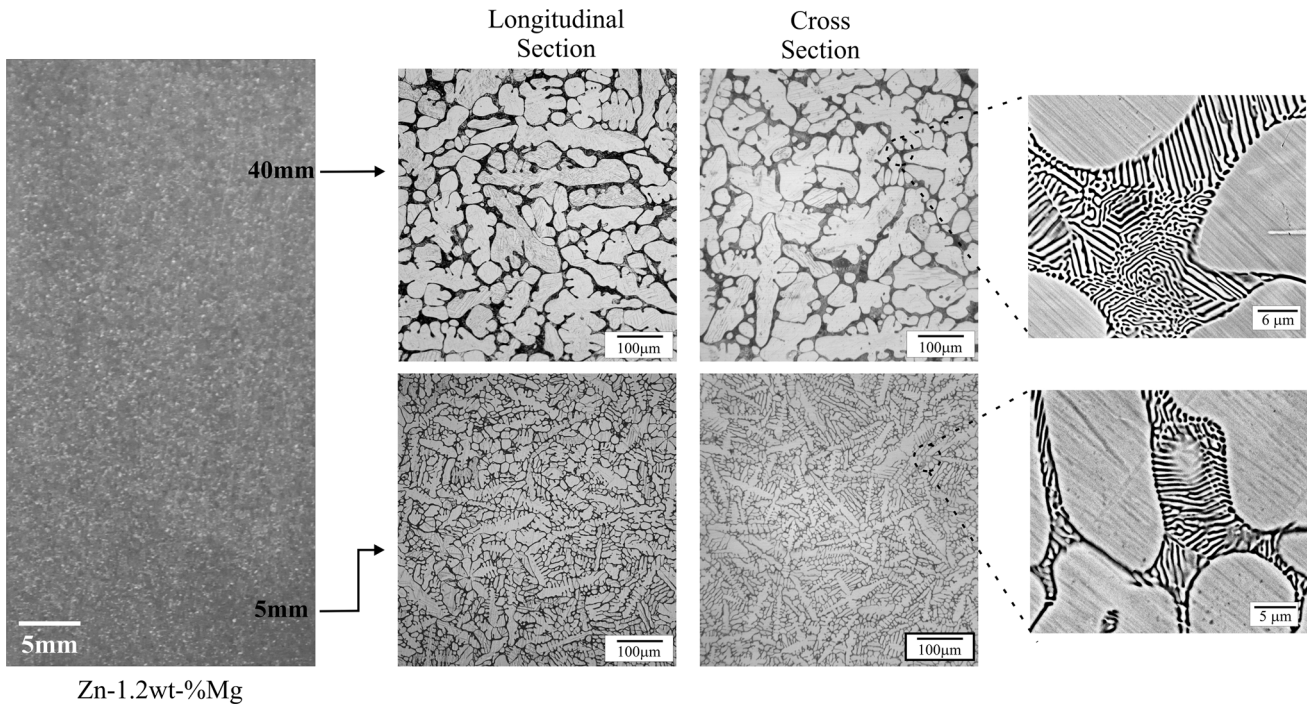


Fig. 10—Macrostructure and typical microstructures along the DS Zn-1.2 wt-pct Mg casting.

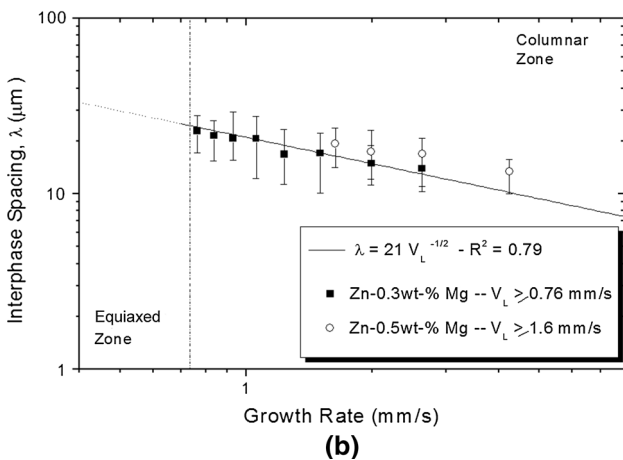
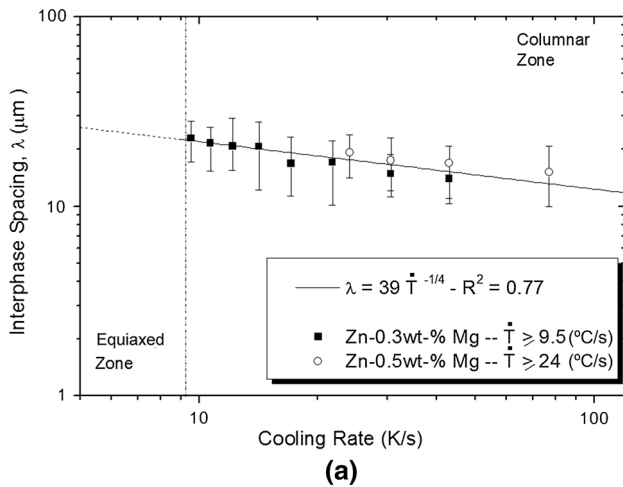


Fig. 11—Interphase spacing of plate-like cells: (a) vs cooling rate; (b) vs growth rate. R^2 is the coefficient of determination.

of the casting, as shown in Figure 10. However, the eutectic morphology is always lamellar along the entire range of experimental cooling rates, no matter the Zn-Mg alloy examined, as can be seen in the SEM images of Figures 8, 9, and 10.

C. Cooling Rate, Growth Rate, and Microstructural Spacings

The interphase spacing (λ) measured from the plate-like cells of the columnar zones of both Zn0.3 wt-pct Mg and Zn0.5 wt-pct Mg castings are plotted in Figure 11 as a function of cooling rate (a) and growth rate (b) with the error bars corresponding to the range of minimum and maximum experimental values. Since this morphology is associated with a higher solidification kinetics regime, Figure 11 also indicates from which V and \dot{T} values such morphology occurs. The growth laws exponents in Figure 11 were found to be $-1/2$ and $-1/4$ for V and \dot{T} , respectively, *i.e.*, the λ vs V correlation is in agreement with the classical Jackson and Hunt equation for the lamellar growth of eutectics: $\lambda^2 V = \text{constant}$.^[66] The $-1/4$ exponent associated with the λ vs \dot{T} correlation (Figure 11(a)) is supported by an analytical heat flow model, which relates V to \dot{T} , where \dot{T} is shown to be given by a constant $\times V^2$ for unidirectional transient solidification conditions of pure metals and binary alloys.^[67,68] It is also curious to remark that the growth law derived in the present study for the growth of plate-like cells of Zn-Mg alloys ($\lambda = 39 \dot{T}^{-1/4}$) is the same experimentally determined for the growth of plate-like cells of Zn-10 wt pct Sn and Zn-20 wt-pct Sn alloys.^[64,65] The same numerical multiplier in the growth law for the alloys of two different alloy systems

(Zn-Mg and Zn-Sn) can be considered an experimental coincidence. However, the $-1/4$ exponent seems to be associated, for these alloys of both systems, with the well-organized microstructures characterized by a coupled growth of alternate Zn-rich plate-like cells/eutectic mixtures, resembling a eutectic-like lamellar growth. Indeed, it was shown, for Zn-Sn alloys that the increase in the solute content to 30 and 40 wt pct Sn led to a transition in the cellular pattern. This has consequential effects in the growth laws, which were shown to have experimental dependences with \dot{T} related to a $-1/2$ exponent that are typically associated with the growth of dendrites and regular cells of binary alloys.^[65]

As mentioned before, along the equiaxed zone of both Zn-0.3 wt-pct Mg and Zn-0.5 wt-pct Mg castings, a gradual morphological microstructural transition takes place (granular Zn-rich matrix > dendritic branches), and no systematic measurements of the microstructure scale can be made. However, the Zn-1.2 wt-pct Mg alloy casting has the Zn-rich matrix formed by equiaxed

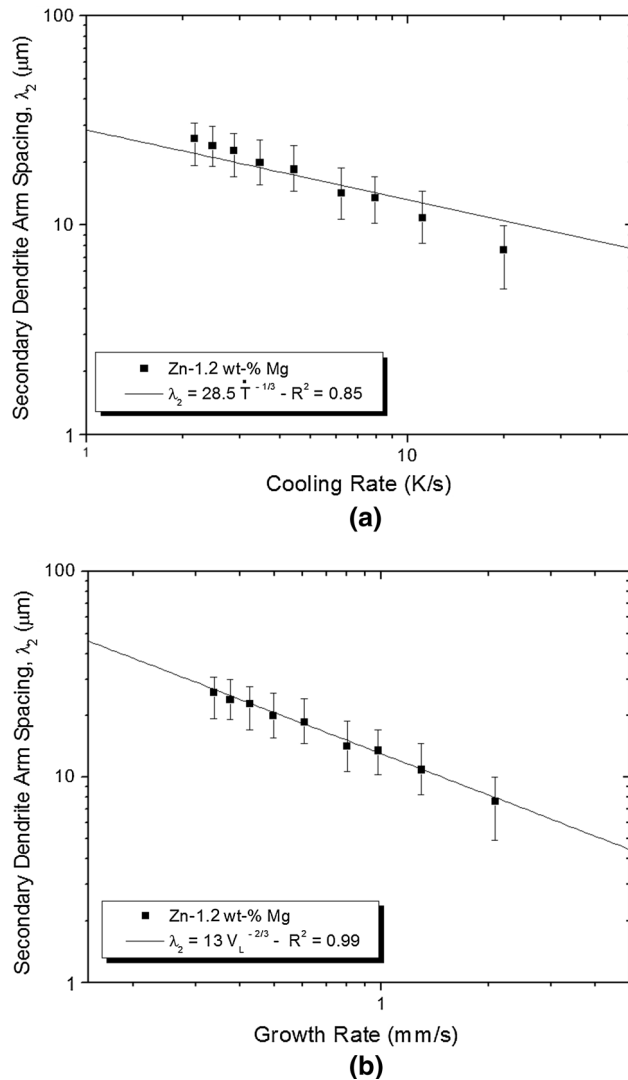


Fig. 12—Secondary dendritic arm spacing: (a) vs cooling rate; (b) vs growth rate. R^2 is the coefficient of determination.

dendritic grains along the entire DS casting. The evolution of the scale of these secondary branches along the casting length is shown in Figure 12, associated with the range of experimental cooling rates and growth rates. It can be seen that $-1/3$ and $-2/3$ exponents are related to \dot{T} and V , respectively. Similar exponents have also been reported for the transient dendritic growth of a number of binary alloys.^[69]

For comparison purposes, results from the literature concerning the evolution of secondary dendrite arm spacing of hypoeutectic Zn-Mg alloys are plotted in Figure 13 with the experimental growth law proposed in Figure 12(a). These results are from studies by Liu and Jones^[35,36] and refer to both steady-state Bridgman growth of Zn-Mg alloy samples at a temperature gradient of 15 K/mm ($0.1 < \dot{T} < 50$ K/s) and at a higher temperature gradient of 95 K/mm achieved by tungsten inert gas (TIG) weld at traverse speeds from 10 to 40 mm/s ($950 < \dot{T} < 3800$ K/s). It can be seen that the experimental points generally conform to the trend of the experimental growth law derived in the present investigation. This reinforces the proper application of the exponent $-1/3$ in order to correlate the evolution of λ_2 with \dot{T} for both steady-state and unsteady-state solidification conditions. A similar conclusion has been recently reported in a comparative study on steady and unsteady-state solidification of hypoperitectic Pb-Bi alloys.^[70]

The evolutions of the eutectic interphase spacing (interlamellar spacing) as a function of cooling rate and growth rate are depicted in Figure 14. It can be seen that the λ_{eut} vs V results conform to the classical Jackson and Hunt equation for the lamellar growth of eutectics: $\lambda^2 V = \text{constant}$.^[66] Considering the microstructures associated with the equiaxed zones of the DS castings, it can be seen that λ_{eut} does not exhibit any significant variation with the alloy Mg content, *i.e.*, similar λ_{eut} vs V and λ_{eut} vs \dot{T} , correlations are established, despite the slight trend of higher λ_{eut} associated with the Zn-1.2 wt-pct Mg alloy. Liu and Jones^[35] reported a similar conclusion for the steady-state growth of Zn-Mg

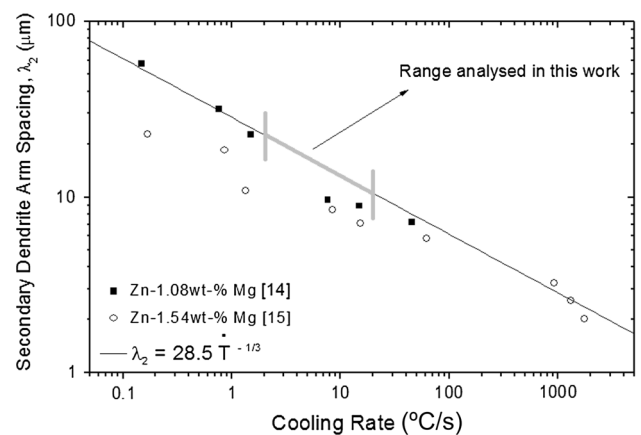


Fig. 13—Secondary dendritic arm spacing as function of cooling rate: growth law derived in the present study for unsteady solidification compared with steady-state experimental results.

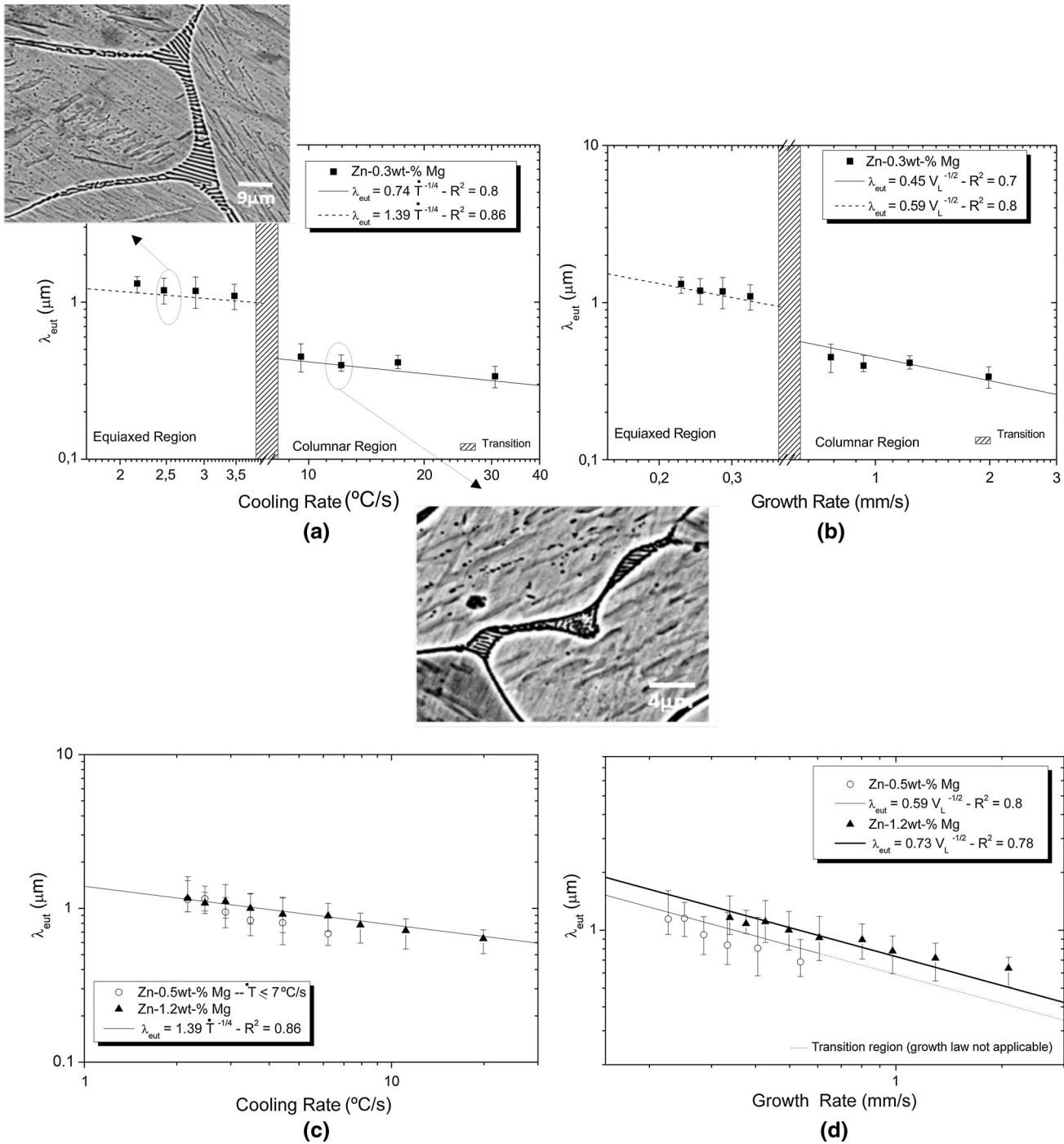


Fig. 14—Eutectic interphase spacing (λ_{eut}) as a function of (a) and (c) cooling rate; (b) and (d) growth rate. R^2 is the coefficient of determination.

alloys in the range 2.45 to 3.48 wt-pct Mg. However, when analyzing the evolution of λ_{eut} in the columnar region of the 0.3 wt-pct Mg casting, it can be seen that λ_{eut} is significantly lower when compared with values measured along the equiaxed zone. It is important to remark that the heat transfer mechanisms associated with growth of an equiaxed nucleus and those of a columnar one are quite different, *i.e.*, differences in the

growth laws associated with these two solidification regimes are expected to occur.

IV. CONCLUSIONS

The following conclusions can be drawn from the present experimental investigation:

- The macrostructures of the DS Zn-Mg castings varied according to the alloy Mg content. The Zn0.3 wt-pct Mg and Zn0.5 wt-pct Mg alloys exhibited columnar zones for cooling rates higher than 9.5 and 24 K/s, respectively. In contrast, the entire DS casting of the Zn-1.2 wt-pct Mg alloy exhibited an equiaxed macrostructure.
- The typical microstructure of the Zn-Mg DS castings was shown to be formed by a Zn-rich matrix and two kinds of competitive eutectic mixture (Zn-Zn₁₁Mg₂ and Zn-Zn₂Mg), which can be observed concurrently all along the DS castings. The morphology of the Zn-rich matrix for the 0.3 wt-pct Mg and 0.5 wt-pct Mg alloys was shown to vary from high-cooling rate plate-like cells (associated with the columnar zones), followed by a microstructural transition along the equiaxed zone, characterized by a granular phase that was progressively being transformed into dendritic-like equiaxed grains. The Zn-1.2 wt-pct Mg DS casting was shown to have a Zn-rich matrix of equiaxed dendritic grains along the entire casting length.
- Experimental growth laws were proposed relating the plate-like cells interphase spacing (λ), the secondary dendritic arm spacing (λ_2), and the eutectic interphase spacing (λ_{eut}) to solidification thermal parameters (cooling rate, \dot{T} and growth rate, V). It was shown that both λ_{eut} vs V and λ vs V results conform to the classical Jackson and Hunt equation for the lamellar growth of eutectics ($\lambda^2 V = \text{constant}$). The experimental growth law λ_2 vs \dot{T} derived in the present study for unsteady solidification was shown to encompass also a wide range of cooling rates and secondary dendrite arm spacings of steady-state solidification of hypoeutectic Zn-Mg alloys.

ACKNOWLEDGMENTS

The authors acknowledge the financial support provided by FAPESP-São Paulo Research Foundation, Brazil (Grants 2012/08494-0, 2013/15478-3, 2013/25452-1, 2013/23396-7, 2014/50502-5), CNPq-The Brazilian Research Council, and CSIC-Spanish National Research Council (Project i-link0944).

REFERENCES

- M. Vlot, R. Bleeker, T. Maalman, and G. Van Peristeyn: *Proceedings of Galvanized Sheet Forum, ILZRO and IZA*, Dusseldorf, 2006.
- S. Sugimaru, S. Tanaka, N. Hikita, H. Ohba, A. Yoshie, and S. Nishida: *Nippon Steel Technol. Rep.*, 2007, vol. 96, pp. 34–8.
- P. Volovitch, C. Allely, and K. Ogle: *Corros. Sci.*, 2009, vol. 51, pp. 1251–62.
- M. Dutta, A.K. Halder, and S.B. Singh: *Surf. Coat. Technol.*, 2010, vol. 205, pp. 2578–84.
- C. Yao, W. Chen, and W. Gao: *Surf. Coat. Technol.*, 2013, vol. 219, pp. 126–30.
- J.H. La, S.Y. Lee, and S.J. Hong: *Surf. Coat. Technol.*, 2014, vol. 259, pp. 56–61.
- C. Yao, Z. Wang, S.L. Tay, and W. Gao: *Surf. Coat. Technol.*, 2014, vol. 260, pp. 39–45.
- J. Duchoslav, R. Steinberger, M. Arndt, T. Keppert, G. Luckeneder, K.H. Stellnberger, J. Hagler, G. Angeli, C.K. Rienen, and D. Stifter: *Corros. Sci.*, 2015, vol. 91, pp. 311–20.
- K. Honda, W. Yamada, and K. Ushioda: *Mater. Trans.*, 2008, vol. 49, pp. 1395–1400.
- T. Prosek, A. Nazarov, U. Bexell, D. Thierry, and J. Serak: *Corros. Sci.*, 2008, vol. 50, pp. 2216–31.
- R. Krieg, A. Vimalanandan, and M. Rohwerder: *J. Electrochem. Soc.*, 2014, vol. 161, pp. C156–61.
- T. Prosek, D. Persson, J. Stoullil, and D. Thierry: *Corros. Sci.*, 2014, vol. 86, pp. 231–8.
- M.S. Azevedo, C. Allély, K. Ogle, and P. Volovitch: *Corros. Sci.*, 2015, vol. 90, pp. 472–81.
- T. Prosek, A. Nazarov, A.L. Gac, and D. Thierry: *Prog. Org. Coat.*, 2015, vol. 83, pp. 26–35.
- X. Wang, H. Lu, X. Li, L. Li, and Y. Zheng: *Trans. Nonferrous Met. Soc. China*, 2007, vol. 17, pp. s122–5.
- J. Gao, S. Wu, L. Qiao, and Y. Wang: *Trans. Nonferrous Met. Soc. China*, 2008, vol. 18, pp. 588–92.
- D. Chen, Y. He, H. Too, Y. Zhang, Y. Jiang, X. Zhang, and S. Zhang: *Int. J. Mol. Med.*, 2011, vol. 28, pp. 343–8.
- S. Cai, T. Lei, N. Li, and F. Feng: *Mater. Sci. Eng. C-Biosci.*, 2012, vol. 32, pp. 2570–77.
- H.R. Bakhsheshi-Rad, M.H. Idris, M.R.A. Kadir, S. Farahany, A.F. Lotfjadi, and A.A. Suhasril: *Adv. Sci. Lett.*, 2013, vol. 19, pp. 2553–7.
- P.R. Cha, H.S. Han, G.F. Yang, Y.C. Kim, K.H. Hong, S.C. Lee, J.Y. Jung, J.P. Ahn, Y.Y. Kim, S.Y. Cho, J.Y. Byun, K.S. Lee, S.J. Yang, and H.K. Seok: *Sci. Rep.*, 2013, vol. 3, p. 2367.
- J. Kubásek and D. Vojtech: *J. Mater. Sci. Mater. Med.*, 2013, vol. 24, pp. 1615–26.
- H.R. Bakhsheshi-Rad, E. Hamzah, A. Fereidouni-Lotfjadi, M. Daroonparvar, M.A.M. Yajid, M. Mezbahul-Islam, M. Kasiri-Asgarani, and M. Medraj: *Mater. Corros.*, 2014, vol. 65, pp. 1178–87.
- D. Liu, Y. Liu, Y. Huang, R. Song, and M. Chen: *Prog. Nat. Sci.*, 2014, vol. 24, pp. 452–7.
- C. Yao, Z. Wang, S.L. Tay, T. Zhu, and W. Gao: *J. Alloys Compd.*, 2014, vol. 602, pp. 101–7.
- M.S. Dargusch, K. Pettersen, K. Nogita, M.D. Nave, and G.L. Dunlop: *Mater. Trans.*, 2006, vol. 47, pp. 977–82.
- E. Zhang, L. Yang, J. Xu, and H. Chen: *Acta Biomater.*, 2010, vol. 6, pp. 1756–62.
- L. Yang, Y. Huang, F. Feyerabend, R. Willumeit, C. Mendis, K.U. Kainer, and N. Hort: *Acta Biomater.*, 2013, vol. 9, pp. 8499–8508.
- G. Bi, Y. Li, S. Zang, J. Zhang, Y. Ma, and Y. Hao: *J. Magnes. Alloys*, 2014, vol. 2, pp. 64–71.
- W.R. Osório, E.S. Freitas, and A. Garcia: *Corrosion*, 2014, vol. 70, pp. 1031–42.
- S. Zhao, Q. Peng, H. Li, and B. Liu: *J. Alloys Compd.*, 2014, vol. 584, pp. 56–62.
- F. Bertelli, C. Brito, I.L. Ferreira, G. Reinhart, H. Nguyen-Thi, N. Mangelinck-Noel, N. Cheung, and A. Garcia: *Mater. Des.*, 2015, vol. 72, pp. 31–42.
- M.T. Mohammed, Z.A. Khan, M. Geetha, and A.N. Siddiquee: *J. Alloys Compd.*, 2015, vol. 634, pp. 272–80.
- Y.L. Zhou, Y. Li, D.M. Luo, Y. Ding, and P. Hodgson: *Mater. Sci. Eng. C-Biosci.*, 2015, vol. 49, pp. 93–100.
- P.R. Goulart, J.E. Spinelli, N. Cheung, and A. Garcia: *Mater. Chem. Phys.*, 2010, vol. 119, pp. 272–8.
- H.Y. Liu and H. Jones: *Acta Metall. Mater.*, 1992, vol. 40, pp. 229–39.
- H.Y. Liu and H. Jones: *J. Mater. Sci. Lett.*, 1992, vol. 11, pp. 769–70.
- P.K. Rohatgi, K. Pasciak, C.S. Narendranath, S. Ray, and A. Sachdev: *J. Mater. Sci.*, 1994, vol. 29, pp. 5357–66.
- D. Bouchard and J.S. Kirkaldy: *Metall. Mater. Trans. B*, 1997, vol. 28B, pp. 651–63.
- K.N. Prabhu and A.A. Ashis: *Mater. Manuf. Process*, 2002, vol. 17, pp. 469–81.

40. S. Louhenkilpi, M. Mäkinen, S. Vapalahti, T. Räisänen, and J. Laine: *Mater. Sci. Eng. A-Str.*, 2005, vols. 413–414, pp. 135–38.
41. H.M. Şahin, K. Kocatepe, R. Kayikci, and N. Akar: *Energy Convers. Manage.*, 2006, vol. 47, pp. 19–34.
42. D.S. Sui and Z.S. Cui: *Trans. Nonferrous Mater. Soc. China*, 2008, vol. 18, pp. 399–404.
43. P.R. Goulart, J.E. Spinelli, N. Cheung, I.L. Ferreira, and A. Garcia: *J. Alloys Compd.*, 2009, vol. 470, pp. 589–99.
44. A. Kumar and P. Dutta: *J. Mater. Sci.*, 2009, vol. 44, pp. 3952–61.
45. M. Amoozraei, S. Gurevich, and N. Provatas: *Acta Mater.*, 2010, vol. 58, pp. 6115–24.
46. E. Hajjari, M. Divandari, S.H. Razavi, S.M. Emami, and S. Kamado: *Appl. Surf. Sci.*, 2011, vol. 257, pp. 5077–82.
47. W.R. Osório, J.E. Spinelli, N. Cheung, and A. Garcia: *Mater. Sci. Eng. A-Struct.*, 2006, vol. 420, pp. 179–86.
48. M. Dias, T. Costa, O. Rocha, J.E. Spinelli, N. Cheung, and A. Garcia: *Mater. Character.*, 2015, vol. 106, pp. 52–61.
49. N.C. Verissimo, C. Brito, W.R.L. Santos, N. Cheung, J.E. Spinelli, and A. Garcia: *J. Alloys Compd.*, 2016, vol. 662, pp. 1–10.
50. C.A. Siqueira, N. Cheung, and A. Garcia: *Metall. Mater. Trans. A*, 2002, vol. 33A, pp. 2107–18.
51. J.A. Spittle: *Int. Mater. Rev.*, 2006, vol. 51, pp. 247–69.
52. A.E. Ares and C.E. Schvezov: *Metall. Mater. Trans. A*, 2007, vol. 38A, pp. 1485–99.
53. Z. Liu, D. Qiu, F. Wang, J.A. Taylor, and M. Zhang: *Mater. Character.*, 2015, vol. 106, pp. 1–10.
54. C. Brito, G. Reinhart, H. Nguyen-Thi, N. Mangelinck-Noël, N. Cheung, J.E. Spinelli, and A. Garcia: *J. Alloys Compd.*, 2015, vol. 636, pp. 145–9.
55. R. Trivedi, J.A. Sekhar, and V. Seetharaman: *Metall. Trans. A*, 1989, vol. 20A, pp. 769–77.
56. W.W. Mullins and R.F. Sekerka: *J. Appl. Phys.*, 1964, vol. 35, pp. 444–51.
57. O.L. Rocha, C.A. Siqueira, and A. Garcia: *Mater. Sci. Eng. A-Struct.*, 2003, vol. 361, pp. 111–8.
58. D. Ma, Y. Li, S.C. Ng, and H. Jones: *Acta Mater.*, 2000, vol. 48, pp. 419–31.
59. D. Ma, Y. Li, S.C. Ng, and H. Jones: *Sci. Technol. Adv. Mater.*, 2001, vol. 2, pp. 127–30.
60. W. Xu, Y.P. Feng, Y. Li, G.D. Zhang, and Z.Y. Li: *Acta Mater.*, 2002, vol. 50, pp. 183–93.
61. W. Xu, Y.P. Feng, Y. Li, and Z.Y. Li: *Mater. Sci. Eng. A-Struct.*, 2004, vol. 373, pp. 139–45.
62. C. Brito, C.A. Siqueira, J.E. Spinelli, and A. Garcia: *Mater. Lett.*, 2012, vol. 80, pp. 106–9.
63. M. Dias, C. Brito, F. Bertelli, and A. Garcia: *Mater. Chem. Phys.*, 2014, vol. 143, pp. 895–9.
64. W.L.R. Santos, C. Brito, J.M.V. Quaresma, J.E. Spinelli, and A. Garcia: *Mater. Sci. Eng. B-Solid.*, 2014, vol. 182, pp. 29–36.
65. W.L.R. Santos, C. Brito, F. Bertelli, J.E. Spinelli, and A. Garcia: *J. Alloys Compd.*, 2015, vol. 647, pp. 989–96.
66. K.A. Jackson and J.D. Hunt: *Trans. TMS-AIME*, 1966, vol. 236, pp. 1129–42.
67. A. Garcia, T.W. Clyne, and M. Prates: *Metall. Trans. B*, 1979, vol. 10B, pp. 85–92.
68. I.L. Ferreira, C.A. Santos, V.R. Voller, and A. Garcia: *Metall. Mater. Trans. B*, 2004, vol. 35B, pp. 285–97.
69. J.E. Spinelli, N. Cheung, and A. Garcia: *Philos. Mag.*, 2011, vol. 91, pp. 1705–23.
70. M.A.P. Castanho, P.R. Goulart, C. Brito, J.E. Spinelli, N. Cheung, and A. Garcia: *Mater. Sci. Technol.*, 2015, vol. 31, pp. 105–13.